Defense Technical Information Center
Compilation Part Notice

ADP014107

TITLE: Prediction of Noise Radiated by a Non-Isothermal Mixing Layer Using a Low Mach Number Approximation

DISTRIBUTION: Approved for public release, distribution unlimited
Availability: Hard copy only.

This paper is part of the following report:

TITLE: Aging Mechanisms and Control. Symposium Part A - Developments in Computational Aero- and Hydro-Acoustics. Symposium Part B - Monitoring and Management of Gas Turbine Fleets for Extended Life and Reduced Costs [Les mecanismes vieillissants et le controle] [Symposium Partie A - Developpements dans le domaine de l'aeroacoustique et l'hydroacoustique numeriques] [Symposium Partie B ...

To order the complete compilation report, use: ADA415749

The component part is provided here to allow users access to individually authored sections of proceedings, annals, symposia, etc. However, the component should be considered within the context of the overall compilation report and not as a stand-alone technical report.

The following component part numbers comprise the compilation report:
ADP014092 thru ADP014141

Prediction of Noise Radiated by a Non-Isothermal Mixing Layer Using a Low Mach Number Approximation

F. Golanski, V. Fortuné and E. Lamballais
Laboratoire d'Études Aérodynamiques
Bâtiment H
40, avenue du recteur Pineau
86022 POITIERS CEDEX, France

Abstract

The ability of an acoustic analogy to predict the sound radiated by a transitional mixing layer is evaluated by means of Direct Numerical Simulation results. The specific case of low Mach number flows with density variations is investigated. We consider the strategy where the acoustic source information is based on numerical results where the sound waves has been removed in order to limit the global computational cost of the prediction. It is shown that the low Mach number approximation coupled to the acoustic analogy can lead to very accurate predictions for the radiated sound if the acoustic sources in Lighthill's equation are taken into account carefully. The scaling laws of the acoustic intensity deduced from a repeated use of the Lighthill's analogy on a wide range of Mach numbers suggest a new interpretation about the experimental observations on the sound emission from hot and cold jets.

1   Introduction

A better control of the noise radiated by turbulence is required in many industrial applications. The improvement of sound prediction tools needs to study the sound generation and propagation, the main goal of the aeroacoustics. The far field sound can be predicted with the aid of a computer, with mainly two different numerical strategies. The first one consists in the explicit computation of the sound on a very large computational domain by solving the compressible Navier-Stokes equations in the context of the Direct Numerical Simulation (DNS). The direct access of the far acoustic field offered by this approach is clearly very attractive, but the direct sound calculation is still too expensive and problematic (boundary condition treatment) for turbulent flows in non-academic geometry. A second point is that for low Mach number applications, even for very simple flows, the computational cost is dramatically increased due to the numerical difficulties to consider simultaneously the turbulent fluctuations and the very fast and low amplitude acoustic phenomena. Hence, in our knowledge, no direct sound computation results using DNS at low Mach number are available in computational aeroacoustics except for very simple flow geometry [15, 7, 8]. An alternative method of far-field sound prediction is to use an acoustic analogy coupled to a near-field calculation (in the acoustic source zone) using DNS or Large Eddy Simulation (LES). In such an hybrid method, since simulation of the flow is necessary only in the region where the source terms are significant, the computational cost requirement is strongly decreased. The use of acoustic analogy in this context has been validated in previous studies [3, 7, 2, 15, 9, 8] by comparison between direct sound computation and its estimation by solving the Lighthill's equation. A crucial question in the use of acoustic analogy concerns the accuracy requirement for the acoustic source computation. Hence, a crude approximation of the acoustic sources can lead to wrong sound predictions. The more straightforward method to compute the near-field including acoustic sources is to solve directly the compressible Navier-Stokes equations at the Mach number of the flow under study. However, for low Mach number applications, even if the computational domain is limited to the active source region, such a compressible DNS/LES remains very expensive. In order to avoid this drawback, a second opportunity is to perform a DNS/LES based on governing equations where the sound waves are removed. The most common use is to consider the incompressible Navier-Stokes equations for isothermal flows, but an equivalent removal of sound waves can be obtained for non-isothermal applications in solving the low Mach number approximate
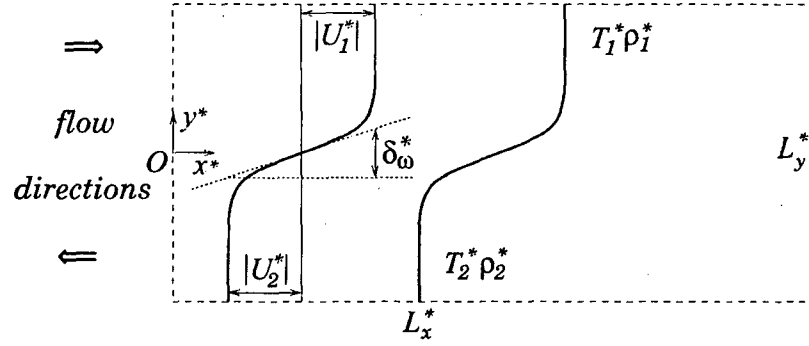
Figure 1: The temporal mixing layer flow configuration.

Navier-Stokes equations. Since the sound is removed from such DNS/LES results, it must be restored in the region of interest using the acoustic analogy. In this paper, we want to evaluate this strategy of sound removal/restoration in the context of a transitional non-isothermal flow. We first concentrate our attention on the acoustic source computation and their treatment in the acoustic analogy stage. Finally, scaling laws of acoustic intensity with the Mach number are discussed by varying the Mach number in the frame of the acoustic analogy.

2 Flow configuration

In this work, we consider the temporal development of a two-dimensional mixing layer between two streams of velocity, temperature and density noted respectively (U_1^*, T_1^*, ρ_1^*) and (U_2^*, T_2^*, ρ_2^*) in a rectangular domain of dimensions $L_x^* \times L_y^*$ (see figure 1 for more details about the flow and domain geometries). Note that throughout this paper, dimensional quantities are indicated by a superscript *. The flow is assumed to be periodic in the streamwise direction x^* while free-slip boundary conditions are imposed at $y^* = \pm L_y^*/2$. The initial pressure p^* is assumed to be constant. The initial mean velocity field is given by the following hyperbolic-tangent profile

$$\langle u^* \rangle (y^*) = \frac{U_1^* + U_2^*}{2} + \frac{U_1^* - U_2^*}{2} \tanh\left(\frac{2y^*}{\delta_\omega^*}\right) \tag{1}$$

where δ_ω^* is the initial vorticity thickness while the operator $\langle . \rangle$ indicates an average over the streamwise direction x^*. U_1^* and U_2^* are determined in order to verify the condition $U_c^* = 0$ where U_c^* is the convection velocity of the large scale structures [1] with

$$U_c^* = \frac{\sqrt{T_1^*}U_2^* + \sqrt{T_2^*}U_1^*}{\sqrt{T_1^*} + \sqrt{T_2^*}} \tag{2}$$

The initial temperature is deduced using the Crocco-Buseman relation

$$\begin{aligned}
T^*(y^*) &= \frac{1}{2c_p^*}\left[-\langle u^* \rangle^2(y^*) - U_1^* U_2^* + \langle u^* \rangle (y^*)(U_1^* + U_2^*)\right] \\
&+ (T_1^* - T_2^*)\frac{\langle u^* \rangle (y^*)}{U_1^* - U_2^*} + \frac{T_2^* U_1^* - T_1^* U_2^*}{U_1^* - U_2^*}
\end{aligned} \tag{3}$$

In order to destabilize the flow, an incompressible disturbance field $(\tilde{u}^*, \tilde{v}^*)$ is added to the mean velocity. The vertical velocity perturbation is composed of a fundamental and two sub-harmonic disturbances such as

$$\tilde{v}^*(x^*, y^*) = A^* e^{-\sigma\left(\frac{y^*}{\delta_\omega^*}\right)^2}\left[\cos\left(\frac{8\pi}{L_x^*}x^*\right) + \frac{1}{8}\cos\left(\frac{4\pi}{L_x^*}x^*\right) + \frac{1}{16}\cos\left(\frac{2\pi}{L_x^*}x^*\right)\right] \tag{4}$$

with $A^* = 0.025\,(U_1^* - U_2^*)$, and $\sigma = 0.05$. Since this set of initial conditions corresponds exactly to the one used in [7], a detailed comparison with one simulation referenced in this previous study will be given in the section 7.

3   Conservation laws

We consider a perfect gas flow governed by the following equations written in nondimensional form

$$\frac{\partial \rho}{\partial t} + \frac{\partial \rho u_i}{\partial x_i} = 0 \tag{5}$$

$$\frac{\partial \rho u_i}{\partial t} + \frac{\partial \rho u_i u_j}{\partial x_j} = -\frac{\partial p}{\partial x_i} + \frac{1}{Re}\frac{\partial \tau_{ij}}{\partial x_j} \tag{6}$$

$$\frac{\partial E}{\partial t} + \frac{\partial (p+E)u_j}{\partial x_j} = \frac{1}{Re}\frac{\partial u_i \tau_{ij}}{\partial x_j} + \frac{1}{M^2 Re Pr(\gamma-1)}\frac{\partial^2 T}{\partial x_j^2} \tag{7}$$

$$p = \frac{\rho T}{\gamma M^2} \tag{8}$$

in a Cartesian coordinates $x_i = (x, y, z)$ where $u_i = (u, v, w)$ are the velocity components, p and ρ being respectively the pressure and density fields. All variables are nondimensionalized using δ_ω^* as reference length, $U_1^* - U_2^*$ as reference velocity, ρ_2^* as reference density and T_2^* as reference temperature. Here, $\gamma = c_p^*/c_v^*$ is the ratio of specific heats while the universal gas constant is noted $r^* = c_p^* + c_v^*$. The three fundamental nondimensional parameters are the Reynolds number $Re = \rho_2^*(U_1^* - U_2^*)\delta_\omega^*/\mu^*$, the Prandtl number $Pr = \mu^* c_p^*/k^*$ and the Mach number $M = (U_1^* - U_2^*)/\sqrt{\gamma r^* T_2^*}$, where both the dynamic viscosity μ^* and the thermal conductivity k^* are assumed to be constant. The viscous stress tensor is given by

$$\tau_{ij} = \frac{\partial u_i}{\partial x_j} + \frac{\partial u_j}{\partial x_i} - \frac{2}{3}\frac{\partial u_k}{\partial x_k}\delta_{ij} \tag{9}$$

while the total energy per unit volume is expressed by

$$E = \frac{p}{\gamma - 1} + \frac{1}{2}\rho\, u_i u_i. \tag{10}$$

These equations, usually refereed as the compressible Navier-Stokes equations, allow to describe the motion of a perfect gas in a wide range of Mach numbers by considering simultaneously the vortical, entropic and acoustic motions and their eventual coupling.

4   Low Mach number approximation

In many applications, the flow occurs at low speeds. If the fluid velocity is everywhere small compared to the sound speed, it can be clearly an advantage to exploit this feature in order to derive a set of equations easier to solve numerically. The main gain of such approach concerns the computational cost which can be strongly decreased in assuming that the Mach number M is low. More precisely, when the full compressible Navier-Stokes equations are considered, the presence of acoustic waves in the flow impose the use of very small time steps due to the numerical stability of explicit method through the CFL condition. Hence, if the same physical domain and spatial resolution are used, the computational cost of a compressible DNS is in first approximation proportional to M^{-1}. For very low Mach number flows, such a scaling of the computational cost is clearly a drawback, while being mainly conditioned by acoustic phenomena of negligible effects on the flow dynamics. In order to avoid this limitation, it is then very attractive to consider a simplified problem where the acoustic modes are decoupled from the vorticity and entropy modes. The set of equations governing the vorticity and entropy modes can be established by applying a low Mach number approximation to equations (5)−(8). Formally, these simplified equations are derived in introducing a small parameter

$$\varepsilon = \gamma M^2 \tag{11}$$

which is used to expand ρ, u_i and T as

$$\rho = \rho^{(0)} + \varepsilon\rho^{(1)} + \dots \tag{12}$$

$$u_i = u_i^{(0)} + \varepsilon u_i^{(1)} + \dots \tag{13}$$

$$T = T^{(0)} + \varepsilon T^{(1)} + \dots \tag{14}$$

while the state law (8) impose an expansion for p such as

$$p = \frac{p^{(0)}}{\varepsilon} + p^{(1)} + \dots \tag{15}$$

Note that in (15), $p^{(0)}$ and $p^{(1)}$ can be interpreted as nondimensional pressures using respectively $\rho_2^* r^* T_2^*$ and $\rho_2^*(U_2^* - U_1^*)$, so that $p^{(0)}$ is currently called the thermodynamic pressure while $p^{(1)}$ is refereed as the dynamic pressure. Substituting the expansions (12)–(15) into equations (5)–(8) leads to the following system at the lowest order in ε (see [14, 4] for more details)

$$\frac{\partial \rho^{(0)}}{\partial t} + \frac{\partial \rho^{(0)} u_i^{(0)}}{\partial x_i} = 0 \tag{16}$$

$$\frac{\partial p^{(0)}}{\partial x_i} = 0 \tag{17}$$

$$\rho^{(0)} \frac{\partial u_j^{(0)}}{\partial x_j} = \frac{1}{RePrT^{(0)}} \frac{\partial^2 T^{(0)}}{\partial x_j^2} \tag{18}$$

$$p^{(0)} = \rho^{(0)} T^{(0)} \tag{19}$$

Since we consider here an open physical domain, the spatially uniform thermodynamic pressure $p^{(0)}$ is also assumed to be constant in time and fixed to its value at the boundaries $y = \pm L_y/2$ with $p^{(0)} = 1$. In order to close the problem, an additional equation describing the velocity field $u_i^{(0)}$ must be obtained by considering the equation (6) at the zero-order in ε which yields the equation

$$\frac{\partial \rho^{(0)} u_i^{(0)}}{\partial t} + \frac{\partial \rho^{(0)} u_i^{(0)} u_j^{(0)}}{x_j} = -\frac{\partial p^{(1)}}{\partial x_i} + \frac{\partial \tau_{ij}^{(0)}}{\partial x_j} \tag{20}$$

The equations (16), (18), (19) and (20) form a closed system corresponding to a simplification of the Navier-Stokes equations in the frame of the low Mach number approximation. It is important to emphasize that these equations are only asymptotically valid for vanishing Mach number flows, but without any hypothesis about the density variations in space or during the time. Naturally, the assumption $\rho^{(0)} = $ const leads to the conventional incompressible Navier-Stokes equations

$$\frac{\partial u_i^{(0)}}{\partial t} + \frac{\partial u_i^{(0)} u_j^{(0)}}{\partial x_j} = -\frac{\partial P}{\partial x_i} + \frac{1}{Re} \frac{\partial^2 u_i^{(0)}}{\partial x_i^2} \tag{21}$$

$$\frac{\partial u_i^{(0)}}{\partial x_i} = 0 \tag{22}$$

with $P = p^{(1)}/\rho^{(0)}$. An important feature of the low Mach number approximation is that acoustic waves are removed from the derived equations [14]. Hence, this approximation can be viewed as an acoustic filtering procedure which is intrinsic to the derived equations. For low Mach number applications, such a removal of sound waves preserves the flow dynamics in allowing the use of large time step in simulations. In exchange, the ability offered by compressible Navier-Stokes equations to give directly acoustic predictions is loss.

5   Acoustic analogy

5.1   Lighthill's equation

Starting with the equations (5) and (6), the Lighthill's approach [13] consists in deriving a simplified wave equation for ρ such as

$$\frac{\partial^2 \rho}{\partial t^2} - c_\infty^2 \frac{\partial^2 \rho}{\partial x_i^2} = \frac{\partial^2 T_{ij}}{\partial x_i \partial x_j} \tag{23}$$

where the Lighthill's tensor

$$T_{ij} = \underbrace{\rho u_i u_j}_{\text{term 1}} + \underbrace{\left(p - c_\infty^2 \rho\right) \delta_{ij}}_{\text{term 2}} - \underbrace{\frac{1}{Re} \tau_{ij}}_{\text{term 3}} \tag{24}$$

is decomposed here into three terms which are interpreted as the "sources" of the sound waves. The value of c_∞ is the expected nondimensional sound speed in the region where the acoustic waves are considered. Assuming that the source terms are known, the resolution of equation (23) yields a prediction of the acoustic waves corresponding to a given distribution of T_{ij}. Moreover, due to the simplicity of the propagation operator in the left hand side of equation (23), the solution can be expressed analytically with the aid of the Green function formalism. Note that such an approach, refereed as the acoustic analogy, can give reliable information about the sound only in the regions where $T_{ij} \approx 0$, typically in the far acoustic field zone (see [13] for more details).

5.2 Source term treatment

The treatment of the source terms is the key element in the quality of the sound prediction given by the acoustic analogy. For free shear flows, the viscous term 3 can be neglected, even for the low Reynolds number cases considered here [8]. Consequently, this term will no longer be considered in this paper. The term 2 is also frequently omitted by invoking a compensating effect between the pressure and density fluctuations leading to a quasi-constant value for $p - c_\infty^2 \rho$. In fact, such a behaviour can be justified only for isothermal flows where the effects of heat conduction are negligible. More precisely, this last assumption implies that the flow evolution is isentropic with

$$\frac{d\rho}{dt} = \frac{1}{c^2} \frac{dp}{dt} \tag{25}$$

where c is a nondimensional local sound speed with $c^2 = T/M^2$. If in addition the flow evolution is quasi-isothermal, it is reasonable to assume that $c \approx c_\infty$ in the isentropic relation (25) which takes then the simplified form

$$\frac{d}{dt} \left(p - c_\infty^2 \rho \right) \approx 0 \tag{26}$$

Assuming that pressure and temperature fields are simultaneously uniform at one instant, it can be deduced from this last equation that the relation $p - c_\infty^2 \rho \approx \text{const}$ is verified at each time everywhere in the flow. Consequently, in previous works using acoustic analogy, the attention was concentrated mainly on the term 1 assumed to be the dominant contribution in T_{ij}. Naturally, the assumption $c \approx c_\infty$ is not valid in a non-isothermal case and term 2 can no longer be omitted. In a previous work [8], the importance of this term was demonstrated for a non-isothermal flow by analysing DNS results including the direct computation of sound. In the same study, the very small effects of the term 2 on sound emission were also confirmed for an isothermal flow in agreement with the considerations mentioned above.

5.3 Lighthill's equation and low Mach number approximation

In this work, we are interested in the use of an acoustic analogy for low Mach number flows. For isothermal flows, the common use is to determine T_{ij} from an incompressible DNS solving the equations (21),(22) by considering only the term 1 in (24) with $T_{ij} \approx \rho^{(0)} u_i^{(0)} u_j^{(0)}$. The knowledge of T_{ij} allows then to solve in a second step the equation (23) by choosing a relevant value for c_∞. The natural choice is $c_\infty = \sqrt{T/M^2}$ where T and M are respectively the nondimensional temperature and Mach number corresponding to the flow that is under study. In this work, we propose to generalize such an approach to the case of non-isothermal flows (with large density variations) by using the formalism of the low Mach number approximation. For such a purpose, it is worth to substitute the expansions (12)–(15) into the definition (24) in order to evaluate *a priori* the contribution of each flow variable to the lowest orders in ε. Before doing this, it is important to express the value of c_∞ as a function of the flow parameters with

$$c_\infty^2 = \frac{T_\infty}{M^2} \tag{27}$$

$$= \frac{\gamma T_\infty}{\varepsilon} \tag{28}$$

where T_∞ is the nondimensional constant temperature where the sound is predicted. Thus, the expansion of T_{ij} truncated to zero-order in ε yields the following expression

$$T_{ij} = \underbrace{\rho^{(0)}u_i^{(0)}u_j^{(0)}}_{\text{term 1}} + \underbrace{\underbrace{\frac{1}{\varepsilon}\left(p^{(0)} - \gamma T_\infty \rho^{(0)}\right)\delta_{ij}}_{\text{term 2a}} + \underbrace{\left(p^{(1)} - \gamma T_\infty \rho^{(1)}\right)\delta_{ij}}_{\text{term 2b}}}_{\text{term 2}} + \ldots \qquad (29)$$

This relation suggests clearly how results obtained in the frame of the low Mach number approximation must be used in order to estimate T_{ij}. Thus, it can be observed that only the terms 1 and 2a can be deduced from such results due to the presence of $\rho^{(1)}$ in term 2b which is not considered in equations (16),(18),(19) and (20). The non-isothermal character of the flow can however be partially taken into account through the inhomogeneities of $\rho^{(0)}$ in term 2a. An important remark is that the term 2a is the lowest order term in ε. Consequently, it can be expected that this term become dominant for very low Mach number flows even if the density variations $\rho^{(0)}$ are moderate. The contribution of the terms 2a and 2b can be studied *a priori* by considering the relation (25) at the two lowest orders in ε. Thus, it is easy to show that isentropic condition implies

$$\frac{d\rho^{(0)}}{dt} = 0 \qquad (30)$$

for the terms in ε^{-1} and

$$\frac{d}{dt}\left(p^{(1)} - \gamma T^{(0)}\rho^{(1)}\right) = 0 \qquad (31)$$

at zero-order. In the isothermal case where $\rho^{(0)}$ and $T^{(0)}$ are strictly constant (contrary to the compressible variables ρ and T which conserve small variations), the term 2a automatically vanishes while the condition (31) with $T^{(0)} = T_\infty$ shows that the term 2b is conserved following the motion. All these points will be discussed using the results presented in the next sections.

To summarize, the present strategy of acoustic prediction in the frame of low Mach number approximation consists first in the resolution of equations (16), (18), (19) and (20) by assuming $\varepsilon \to 0$ followed by the application of acoustic analogy by considering a finite value for ε in equations (28), (23) and (29), ε being fixed in regards to the real Mach number of the application. Naturally, the validity range of ε has an upper limit which is conditioned by the quality of the assumption that compressibility effects on the real flow dynamics can be neglected.

5.4 Formulation of Lighthill's equation in temporal configuration

The present use of a periodic condition in the streamwise direction allows to consider a simplified flow configuration where the far acoustic field is easily accessible. Hence, due to the unlimited extent of the acoustic source in the x-direction, there is no far field in this direction and the acoustic wave propagation occurs mainly in the y-direction. More precisely, using the average operator $\langle . \rangle = (1/L_x)\int_0^{L_x}(.)dx$, it is possible to show that outside the active region of the flow, the mean part $\langle \phi \rangle$ of any flow variable ϕ travels with the local speed of sound c_∞ as a non-decaying plane wave, formally

$$\langle \phi \rangle = \langle \phi \rangle(y - c_\infty t), \qquad (32)$$

while the disturbance $\phi' = \langle \phi \rangle - \phi$ suffers a $1/\sqrt{y}$ decay [11]. Note that the relation (32) can be verified even if the disturbance ϕ' is not negligible. Consequently, it can be stated that the far acoustic field is only composed of plane acoustic waves which are accessible by considering the mean quantities $\langle \phi \rangle$ at a distance $|y|$ from the shear zone where the condition (32) is verified. In practice, previous works [11, 7] have shown that this critical distance is moderate. For the present study, the mean acoustic quantities are predicted at the location $y = -30$, at a distance from the mixing layer center which is considered to be large enough to verify the condition (32) and consequently to have access to the far-field data.

Denoting the acoustic density as the density deviation from its ambient value in the prediction region, it is easy to express a specific formulation of Lighthill's equation verified by the corresponding mean quantity $\langle \rho - \rho_\infty \rangle$

$$\frac{\partial^2}{\partial t^2}\langle \rho - \rho_\infty \rangle - c_\infty^2 \frac{\partial^2}{\partial y^2}\langle \rho - \rho_\infty \rangle = \frac{\partial^2}{\partial y^2}\langle T_{yy} \rangle \qquad (33)$$

with

$$\langle T_{yy} \rangle = \underbrace{\langle \rho v^2 \rangle}_{\langle T_{yy} \rangle_1} + \underbrace{\langle p - c_\infty^2 \rho \rangle}_{\langle T_{yy} \rangle_2} \tag{34}$$

where the viscous term is omitted for clarity. In this paper, we will consider only this simplified form of the Lighthill's equation where only the knowledge of contributions on mean Lighthill's tensor component $\langle T_{yy} \rangle$ is required. Using the Green's function formalism and after some analytical developments [6], the solution to equation (33) can be written as

$$\langle \rho - \rho_\infty \rangle(y, t) = \underbrace{\frac{1}{2c_\infty^2} \int_{-\infty}^{+\infty} \frac{\partial}{\partial y'} \langle T_{yy} \rangle_1 \left(y', t - \frac{|y - y'|}{c_\infty} \right) dy'}_{\langle \rho - \rho_\infty \rangle_1}$$

$$+ \underbrace{\frac{1}{2c_\infty^2} \int_{-\infty}^{+\infty} \frac{\partial}{\partial y'} \langle T_{yy} \rangle_2 \left(y', t - \frac{|y - y'|}{c_\infty} \right) dy' + \frac{1}{2}(\rho_1 + \rho_2) - \rho_\infty}_{\langle \rho - \rho_\infty \rangle_2} \tag{35}$$

where $\langle \rho - \rho_\infty \rangle_1$ and $\langle \rho - \rho_\infty \rangle_2$ are the contributions of the source terms $\langle T_{yy} \rangle_1$ and $\langle T_{yy} \rangle_2$ on the solution. The constant factor $\frac{1}{2}(\rho_1 + \rho_2) - \rho_\infty$ in (35) is due to boundary terms at $y = \pm\infty$ associated to mean density gradient across the mixing layer (see [6] for more details). By convention, this factor is included in $\langle \rho - \rho_\infty \rangle_2$ in order to bring together the specific non-isothermal contributions. Finally, note that the spatial integration required in the solution (35) was numerically performed in this study by neglecting the contribution of the source terms outside of the y-range of the computational domain $[-L_y/2, +L_y/2]$.

6 Numerical methodology

The evolution equations numerically solved are

$$\frac{\partial \rho^{(0)}}{\partial t} = F_\rho \tag{36}$$

$$\frac{\partial \rho^{(0)} u_i^{(0)}}{\partial t} = -\frac{\partial p^{(1)}}{\partial x_i} + F_{u_i} \tag{37}$$

with

$$F_\rho = -u_j^{(0)} \frac{\partial \rho^{(0)}}{\partial x_j} - \frac{1}{RePrT^{(0)}} \frac{\partial^2 T^{(0)}}{\partial x_j^2} \tag{38}$$

$$F_{u_i} = \frac{\partial}{\partial x_j} \left(\tau_{ij}^{(0)} - \rho^{(0)} u_i^{(0)} u_j^{(0)} \right) \tag{39}$$

Note that in this work, following the technique proposed by [14], we solve a specific form of the density equation (36) which is a combination of the equations (16) and (19). The equations (36) and (37) are integrated in time using a Runge-Kutta scheme except for the pressure term in (37) which requires a specific treatment. More precisely, the discrete integration of these equations on a sub-time step from t_k to t_{k+1} gives

$$\frac{\left(\rho^{(0)} \right)^{k+1} - \left(\rho^{(0)} \right)^k}{\Delta t} = \alpha_k F_\rho^k + \beta_k F_\rho^{k-1} \tag{40}$$

$$\frac{\left(\rho^{(0)} u_i^{(0)} \right)^{k+1} - \left(\rho^{(0)} u_i^{(0)} \right)^k}{\Delta t} = -\frac{\partial \tilde{p}^{(1)}}{\partial x_i} + \alpha_k F_{u_i}^k + \beta_k F_{u_i}^{k-1} \tag{41}$$

with

$$\tilde{p}^{(1)} = \frac{1}{\Delta t} \int_{t_k}^{t_{k+1}} p^{(1)} dt \tag{42}$$

The present Runge-Kutta scheme having four sub-time step, we have $k = 1, 2, 3, 4$ with $t_1 = t_n$ and $t_5 = t_{n+1}$, $\Delta t = t_{n+1} - t_n$ being the full time step. The coefficients α_k and β_k are chosen to satisfy a fourth-order accuracy in time. Since $\tilde{p}^{(1)}$ is not known *a priori*, the equation (41) is fractioned into two steps

$$\frac{\left(\rho^{(0)}u_i^{(0)}\right)^* - \left(\rho^{(0)}u_i^{(0)}\right)^k}{\Delta t} = \alpha_k F_{u_i}^k + \beta_k F_{u_i}^{k-1} \tag{43}$$

$$\frac{\left(\rho^{(0)}u_i^{(0)}\right)^{k+1} - \left(\rho^{(0)}u_i^{(0)}\right)^*}{\Delta t} = -\frac{\partial \tilde{p}^{(1)}}{\partial x_i} \tag{44}$$

Taking the divergence of (44) and using the continuity equation (16), we can obtain a Poisson equation for $\tilde{p}^{(1)}$

$$\frac{\partial^2 \tilde{p}^{(1)}}{\partial x_i \partial x_i} = \frac{1}{\Delta t}\left(\frac{\partial}{\partial x_i}\left(\rho^{(0)}u_i^{(0)}\right)^* - \frac{\partial}{\partial x_i}\left(\rho^{(0)}u_i^{(0)}\right)^{k+1}\right), \tag{45}$$

$$= \frac{1}{\Delta t}\left(\frac{\partial}{\partial x_i}\left(\rho^{(0)}u_i^{(0)}\right)^* + \left(\frac{\partial \rho^{(0)}}{\partial t}\right)^{k+1}\right) \tag{46}$$

The computation of the density time derivative on the right hand side of the equation (46) can be performed using various explicit or implicit approximations [4]. In preliminary calculations, we tested several low- and high-order temporal schemes and we found that the somewhat crude approximation deduced from equation (36)

$$\left(\frac{\partial \rho^{(0)}}{\partial t}\right)^{k+1} = F_\rho^k + O(\Delta t) \tag{47}$$

is the more stable one, allowing the use of large time step while giving reliable results (see following sections).

For spatial discretization, all the spatial derivatives in equations (38),(39) and (46) are computed with the aid of centered compact finite difference schemes of sixth-order accuracy [10]. The computational grid is regular in a non-staggered configuration.

7 Results

7.1 Simulation parameters

The size of the computational domain $(L_x, L_y) = (30.7, 60)$, the ratio of densities $\rho_2/\rho_1 = 2$ and the fundamental parameters ($Re = 400$, $Pr = 0.75$) correspond exactly to a computational configuration referenced in the compressible study [7], as well as the number of grid points in the x-direction with $n_x = 256$. Contrary to this previous work, we do not use here a stretched grid in the y-direction. Since we want to ensure a comparable precision of present results with respect to the data of [7], the resolution in the y-direction was chosen in order to correspond to the resolution used in [7] near $y = 0$ (where the concentration of grid points is maximal) with $\Delta y = 0.12$ which leads to the choice $n_y = 501$. Finally, note that the isothermal case was also considered but will not be presented in details in this paper because all conclusions given in the following about the agreement between present results and previous data of [7] are preserved when $\rho_2/\rho_1 = 1$. Isothermal results will only be shortly considered in the section 7.4 in order to distinguish the isothermal and non-isothermal acoustic emission in terms of scaling laws.

7.2 Instantaneous field analysis

The validity of an acoustic prediction in the frame of low Mach number approximation is naturally conditioned by the validity of the assumption that compressibility effects are negligible on the flow dynamics. In order to verify this hypothesis, visualizations of vorticity and density fields are shown on figures (2) and (3) where present data $\omega_z^{(0)}$ and $\rho^{(0)}$ are compared with their compressible counterpart

ω_z and ρ obtained by [7] at $M = 0.2$. Only the near fields are presented, in the region where source terms are *a priori* significant. The five instants presented allow to observe the formation of four Kelvin-Helmoltz vortices ($t = 24$) followed by two successive pairings ($t = 64$ and $t = 152$). This sequence of transition events is in qualitative agreement with previous DNS results [12]. The remarkable agreement obtained at each time between present results and the compressible data of [7] can be considered as a convincing validation of the numerical methodology used here. It confirms also that at least up to $M = 0.2$, the compressibility do not play a significant part in the flow evolution. Note that the generation of counter-rotating vorticity, an important feature of the transition mechanisms in non-isothermal mixing layers, is very well recovered here, confirming the ability of our numerical code to describe accurately the variable density effects. Since the near fields seem to be well computed, it is reasonable to hope that present data can be used to deduce the correct source terms leading to an accurate prediction of sound. This question will be addressed in the next section.
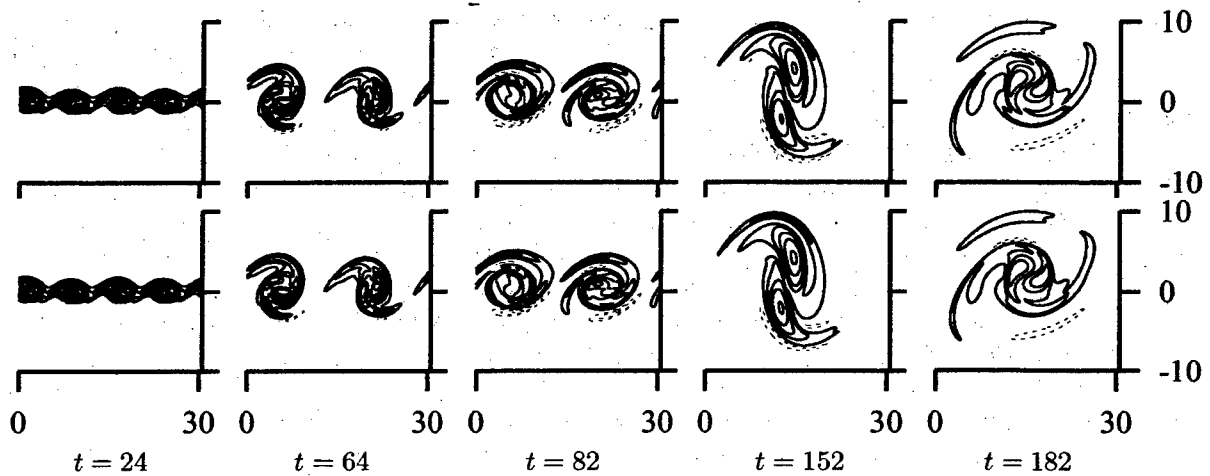

Figure 2: Comparison of vorticity isocontours obtained from present low Mach number approximate DNS ($\omega_z^{(0)}$, bottom) and from a compressible DNS of [7] at $M = 0.2$ (ω_z, top). The contour lines are plotted at intervals of ± 0.01, the dashed lines indicate positive contours (counter-rotating vorticity).
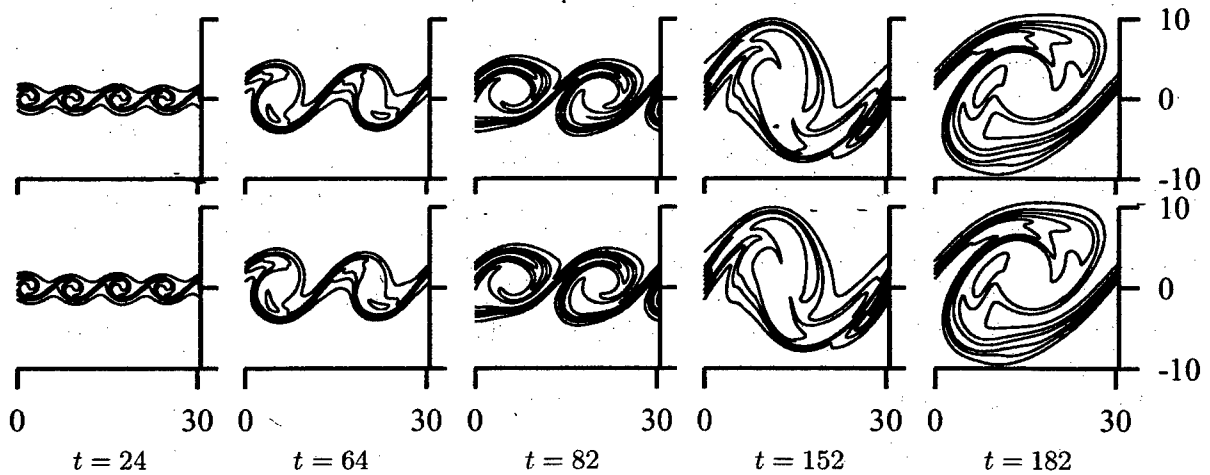

Figure 3: Comparison of density isocontours obtained from present low Mach number approximate DNS ($\rho(0)$, bottom) and from a compressible DNS of [7] at $M = 0.2$ (ρ, top). The contour lines are plotted at intervals of 0.1 from 0.5 to 1.

7.3 Source term analysis

Using the Lighthill's analogy in its temporal formulation for a similar mixing layer, a remarkable agreement was found by [7] between the direct computed sound and its estimation from the solution (35). However, it was emphasized in this study that such an agreement was possible in non-isothermal cases only when the temperature inhomogeneities were taken into account accurately in the two source terms $\langle T_{yy}\rangle_1$ and $\langle T_{yy}\rangle_2$ in (35). Note that since these previous results are fully compressible, the determination of the Lighthill's tensor was obvious. For present results, the compressible component of the motion being not computed, the situation is more delicate. Hence, it is clear that a simple substitution of ρ by $\rho^{(0)}$, u_i by $u_i^{(0)}$ and p by $p^{(1)}$ in the definition (24) of T_{ij} do not lead to a relevant prediction of sound. This point has already been mentioned in the section 5.3 where the development (29) of T_{ij} in ε shows that for the term 2, at zero-order in ε, $p^{(1)}$ is linked to $\rho^{(1)}$ instead of $\rho^{(0)}$, the contribution of $\rho^{(0)}$ being "amplified" by a factor $1/\varepsilon$ compared to the other contributions.

Since $\rho^{(1)}$ is not computed in present low Mach number approximate DNS, we propose here to neglect the term 2b in the approximation (29) of T_{ij}. Note that this assumption can not be justified using a simple argument about the low value of the Mach number because the order in ε of term 2b is the same than for the term 1. The solution obtained from (35) using this assumption is however shown on figure 4 where the time evolution of the mean acoustic density $\langle \rho - \rho_2 \rangle$ at $y = -L_y/2$ is plotted. At this location, the ambient quantities are $\rho_\infty = \rho_2$, $c_\infty = c_2$ and $T_\infty = T_2$. The time scale is shifted by $t_d = t - L_y/(2c_2)$, this correction corresponding to the time necessary for a wave to travel from $y = 0$ to $y = -L_y/2$ at the local sound speed $c_2 = \sqrt{T_2}/M$. On the same figure, the separated contributions of term 1 and term 2 are shown as well. The corresponding estimations of $\langle \rho - \rho_2 \rangle$ using the fully compressible data already performed by [7] at $M = 0.2$ are also given for comparison. Physically, the time variation of the acoustic density $\langle \rho - \rho_2 \rangle$ is due to the sound emission from the shear layer. More precisely, it has been shown by [7] that mainly three acoustic waves are generated during the transition of a 2D temporal mixing layer, each sound emission being consecutively generated by the roll-up and the two successive pairings of the large scale structures. It was also found by the same authors that the second pairing was the noisiest event of the transition in the 2D case. Despite the present approximations on T_{ij}, it is worth to observe that a good agreement is found between the present prediction of acoustic data and their compressible counterpart of [7]. Small though it is, the main difference between these data concerns the term 2. This behaviour is probably related to the lack of the term 2b in the Lighthill's tensor T_{ij} but could also be attributed to a weak Mach number effect on the flow dynamics (to our knowledge, no compressible data about this flow are available for $M < 0.2$). As a first conclusion, we consider here that the low Mach number approximation coupled to the Lighthill's analogy can give a good prediction of the sound radiated by the present non-isothermal flow with a computational cost considerably reduced compared to the fully compressible case. It is interesting to note that when compressible data are used as source terms, the acoustic analogy prediction is valid only for the Mach number considered in the DNS. A prediction at a different Mach number needs to perform again the simulation even if the change of Mach number has very weak effects on the dynamics. The advantage of the low Mach number approximation is that only one simulation is necessary to compute the source terms from which it is possible to deduce acoustic predictions for various Mach numbers. This attractive feature will be exploited in the next section in order to establish numerically the scaling laws followed by the acoustic wave intensities.

7.4 Scaling laws deduced from acoustic analogy

A common method to evaluate the sound level is to consider the acoustic intensity I_{ac} at a given location in the far-field region. In present temporal configuration, this quantity corresponds to the product of the mean acoustic velocity and pressure $I_{ac} = \langle p - p_2 \rangle \langle v \rangle$ evaluated at $y = -L_y/2$. In the acoustic far field, using the assumption that the plane wave propagation in the y-direction is well described by the linearized Euler equations, it is easy to show that the temporal variation of I_{ac} is directly related to the temporal variation of the acoustic density $\langle \rho - \rho_2 \rangle$ with $I_{ac} = -c_2^3 \langle \rho - \rho_2 \rangle^2 /\rho_2$. Note that this relation, very well verified by [7, 6], allows to deduce I_{ac} from the only knowledge of $\langle \rho - \rho_2 \rangle$. In order to study the dependance of I_{ac} with the Mach number, it is interesting to perform an acoustic analogy for a wide range of Mach numbers using the same source terms deduced from the
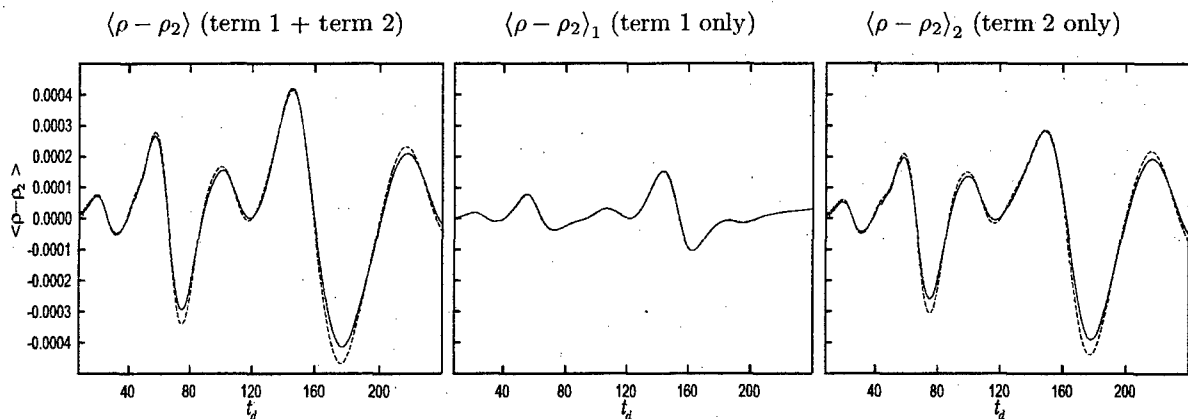
Figure 4: Time evolution of the acoustic density predicted from acoustic analogy applied to compressible DNS results [8] (- - - - -) and to present Mach number approximate results (———).

simulation presented previously. This procedure has been followed in solving 41 times the equation (33) for Mach numbers reparted on the interval $[0.0001, 0.75]$ with a logarithmic distribution. For each given Mach number, the maximum of $|I_{ac}|$ has been determined from the time history of I_{ac} and reported to a diagram $(|I_{ac}|_{\max}, M)$ which is presented on figure 5. The corresponding data deduced from the direct computation of [7] at three different Mach numbers are also given for comparison. Note that for this figure, the acoustic intensity data are nondimentionalized using the local quantities ρ_2 and c_2 (instead of $U_1 - U_2$) in accordance with the common use. Naturally, the excellent agreement of present acoustic predictions with the data of [7] can be observed again on this figure where the isothermal case is also presented. For this last case where $\rho_2/\rho_1 = 1$, the scaling of the maximum acoustic intensity is very well defined over the total range of the Mach number considered with $|I_{ac}|_{\max} \propto \rho_2 c_2^3 \, M^6$. A simple dimensional analysis of the solution (35), assuming the far field relation $\partial/\partial y \approx (1/c_2)\partial/\partial t$ and $T_{ij} = \rho^{(0)} u_i^{(0)} u_j^{(0)}$ allows to find easily this scaling without the accurate computation of the exact source term 1.

In the non-isothermal case, the situation is clearly less simple. Since the balance between the terms 1 and 2a depends on the Mach number, a dimensional analysis can not lead to a single exponent for the scaling of the acoustic intensity. This view is confirmed by the observation of the figure 5 where the acoustic intensity for $\rho_2/\rho_1 = 2$ shows a more sophisticated scaling. For very low Mach numbers, the scaling exponent of the acoustic intensity with the Mach number is around 2. Such a behaviour can be predicted *a priori* in assuming that the Lighthill's tensor can be approximated by $T_{ij} \approx (1/\varepsilon)(p^{(0)} - \gamma T_\infty \rho^{(0)})\delta_{ij}$ which leads to $|I_{ac}|_{\max} \propto \rho_2 c_2^3 \, M^2$. Naturally, the approximation of T_{ij} is valid only if $\varepsilon \ll 1$, that is for very low Mach number. For $M > 0.05$, the explicit solving of (33) shows a clear change in the scaling of I_{ac}, with the approximate scaling law $|I_{ac}|_{\max} \propto \rho_2 c_2^3 \, M^4$ in the range $0.02 < M < 0.2$. For $M > 0.2$, a new change of scaling occurs, but no well defined power law can be identified. Note that for $M > 0.5$, the compressible effects on the flow dynamics become non-negligible, and present acoustic predictions can not be considered as physically valid. Nevertheless, acoustic results are considered here up to $M = 0.75$ in order to better identify the change in the scaling of I_{ac}.

A last comment about the figure 5 concerns the comparison between the isothermal and non-isothermal cases. It is interesting to note that the two different scalings of I_{ac} in isothermal and non-isothermal cases can give a qualitative interpretation of the experimental observations on the sound emissions from cold and hot jets [5]. Hence, for low Mach number, the source of the sound can be essentially attributed to the term 2 and consequently the non-isothermal case is clearly the noisiest one, in agreement with experimental trends for hot and cold jets. However, due to the large value of the scaling exponent in the isothermal case, the increase of the Mach number can lead to a situation where the sound level is stronger in the isothermal case. In cold and hot jet experiments, such an inversion was found to occur around the critical value $M \approx 0.7$. In present results, the corresponding critical value is $M \approx 0.6$, which is outside of the validity range of Mach numbers. Despite this reservation, it is
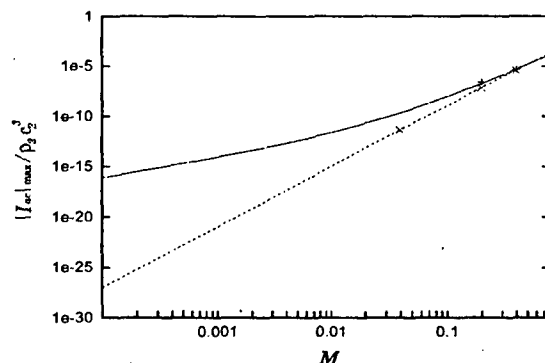
Figure 5: Maximum acoustic intensity versus the Mach number M. Isothermal case $\rho_2/\rho_1 = 1$: present results - - - -, direct computed results of [7] $\times$. Non-isothermal case $\rho_2/\rho_1 = 2$: present results ——, direct computed results of [7] $+$.

worth to observe that this inversion, resulting from a combination between the temperature and Mach number effects, can be understood without the presence of any compressible effects on turbulence, the compressibility being totally missing in present acoustic sources.

References

[1] D. W. Bogdanoff. Compressibility effects in turbulent shear layers. *AIAA Journal*, **21(6)**:926–927, 1983.

[2] T. Colonius and J. B. Freund. Application of Lighthill's equation to a Mach 1.92 turbulent jet. *AIAA Journal*, **38(2)**:368–370, 2000.

[3] T. Colonius, S. K. Lele, and P. Moin. Sound generation in a mixing layer. *J. Fluid Mech.*, **330**:375–409, 1997.

[4] A. W. Cook and J. J. Riley. Direct numerical simulation of a turbulent reactive plume on a parallel computer. *J. Comp. Phys.*, **129**:263–283, 1996.

[5] M. J. Fisher, P. A. Lush, and M. Harper Bourne. Jet noise. *J. Sound Vib.*, **28(3)**:563–585, 1973.

[6] V. Fortuné. *Étude par simulation numérique directe du rayonnement acoustique de couches de mélange isothermes et anisothermes*. PhD thesis, Université de Poitiers, 2000.

[7] V. Fortuné, E. Lamballais, and Y. Gervais. Étude par simulation directe temporelle des effets de la température sur l'émission acoustique des couches de mélange. *C. R. Acad. Sci.*, 328:693–700, 2000.

[8] V. Fortuné, E. Lamballais, and Y. Gervais. Study of temperature effects on radiated noise from mixing layers using DNS. In *7th AIAA/CEAS Aeroacoustics Conference, submitted to AIAA Journal*, Maastricht, The Netherlands, 2001.

[9] J. Freund. Noise sources in a low-Reynolds-number turbulent jet at Mach 0.9. *J. Fluid Mech.*, **438**:277–305, 2001.

[10] S. K. Lele. Compact finite difference schemes with spectral-like resolution. *J. Comp. Phys.*, **103**:16–42, 1992.

[11] S. K. Lele and C. M. Ho. Acoustic radiation from temporally evolving free shear layers. Technical report, Stanford University, 1994.

[12] M. Lesieur, C. Staquet, P. Le Roy, and P. Comte. The mixing layer and its coherence examined from the point of view of two-dimensional turbulence. *J. Fluid Mech.*, **192**:511, 1988.

[13] M. J. Lighthill. On sound generated aerodynamically I. General theory. *Proc. Roy. Soc. A*, **211**:564–587, 1952.

[14] P. A. McMurtry, W. H. Jou, J. J. Riley, and R. W. Metcalfe. Direct numerical simulations of a reacting mixing layer with chemical heat release. *AIAA Journal*, **24(6)**:962–970, 1986.

[15] J. Whitmire and S. Sarkar. Validation of acoustic-analogy predictions for sound radiated by turbulence. *Phys. Fluids*, **12(2)**:381–391, 2000.